IUST
Iran University of Science and Technology

Iranian Journal of Electrical and Electronic Engineering

Journal Homepage: ijeee.iust.ac.ir

Research Paper

An Accurate PMU-Based Fault Location Scheme for Shunt-Compensated Transmission Lines

M. Ahmadinia* and J. Sadeh*(C.A.)

Abstract: In this paper, an accurate fault location scheme based on phasor measurement unit (PMU) is proposed for shunt-compensated transmission lines. It is assumed that the voltage and current phasors on both sides of the shunt-compensated line have been provided by PMUs. In the proposed method, the faulted section is determined by presenting the absolute difference of positive- (or negative-) sequence current angles index, firstly. After determining faulted section, the voltage phasor at the shunt-compensator terminal is estimated via the sound section. The faulted section can be assumed as a perfect transmission line that synchronized voltage and current phasors at one end and voltage phasor at the other end are available. Secondly, a new fault location algorithm is presented to locate the precise fault point in the faulted section. In this algorithm, the location of the fault and the fault resistance are calculated simultaneously by solving an optimization problem, utilizing the heuristic Particle Swarm Optimization (PSO) method. The simulation results in MATLAB/SIMULINK platform demonstrate the high performance of the proposed method in finding the fault location in shunt-compensated transmission lines. The proposed scheme has high accuracy for both symmetrical and asymmetrical fault types and high fault resistance.

Keywords: Fault Location, Shunt-Compensated Transmission Line, Phasor Measurement Unit (PMU), Fault Section Estimation, Partially Data Available, Particle Swarm Optimization.

1 Introduction

POWER systems are continuously exposed to faults in their components. When a fault occurs on a line, the fault should be detected by protection systems as quickly as possible and the faulted line disconnected from the rest of the system. After isolating the faulted line, identifying the accurate fault location is a very significant problem for improving the service reliability [1]. Various methods have been presented for determining the fault point in transmission lines. The proposed methods in [2-7] utilize the data from one end of the line for locating the fault. However, most fault location methods use two-end line data [8-22]. Techniques that utilize voltages and currents from both sides of the line are more efficient than the methods that use information from one side of the line [1].

In some situations, it is necessary to present a method for locating the fault based on complete data of one end of the line and incomplete data of another line end. In other words, in such cases, fault location is done with partial data from line ends [1]. For example, in series- and shunt-compensated lines, even if voltages and currents data are available at both ends of the line, the partial data at the sections' ends are available.

In recent years, utilizing the flexible AC transmission system (FACTS) devices has risen to solve various existing problems in transmission lines. Shunt FACTS devices can increase line power transfer capability by adjusting the midpoint voltage of a line [24]. Considering the simple model for a line, the mid-point of the line is the optimal location for the shunt compensator. However, if the precise model is

Iranian Journal of Electrical and Electronic Engineering, 2021.
Paper first received 05 July 2020, revised 04 March 2021, and accepted 07 April 2021.
* The authors are with the Electrical Engineering Department, Faculty of Engineering, Ferdowsi University of Mashhad, Mashhad, Iran.
E-mails: mohammadreza.ahmadinia@mail.um.ac.ir and sadeh@um.ac.ir.
Corresponding Author: J. Sadeh.
https://doi.org/10.22068/IJEEE.17.4.1927

considered for a line, the shunt compensator must be placed at mid-point or very close to the mid-point of the line to maximize the possible benefits [25-26]. In the presence of equipment such as static VAR compensator (SVC) or static synchronous compensator (STATCOM), the process of phase-detection and impedance measurement does not take place properly; therefore, the conventional fault location methods may encounter some problems [27-28]. Furthermore, if there is a shunt compensator in a line, the line is divided into two shorter lines. Therefore, even if there is data on both ends of the shunt-compensated line, all data from both ends of the two shorter lines are not available. Thus, the accurate location of the fault cannot be determined easily.

Few fault location methods for shunt-compensated transmission lines have been presented in [7, 16, 17, 22]. A fault location method for shunt-compensated double circuit lines based on one-end data is proposed in [7]. The presented methods in [16-17] use two-end data for fault location on shunt-compensated lines. In [16], by using the synchronized both ends data of the line, a new traveling-wave-based fault location method is proposed. The presented method in this paper is non-iterative and can locate the fault without utilizing the shunt-compensator model. Although traveling-wave-based fault location methods are very accurate, these methods require a high sampling rate, and their implementation is very costly [1]. In [17], a fault location method based on unsynchronized two-end data is proposed. The presented scheme in this paper can be used for fault location in the series and shunt compensated lines. However, the presented method in this paper requires series and shunt devices model for locating the fault.

Today, Wide Area Measurement Systems (WAMS) have been widely used to control and monitor power systems [18]. The PMUs, that provided by WAMs, can be utilized for enhancing power system protection, too. In the presented method in [22], two PMUs are located at both sides of the transmission line and synchronized current, and voltage signals are accessible for fault location. In this reference, it is assumed that a PMU is installed at the SVC terminal, and the synchronized data on both ends of the line and SVC terminal are utilized for fault location.

In this paper, an accurate PMU-based fault location scheme for shunt-compensated transmission lines is proposed. In the proposed scheme, two PMUs are located at both sides of shunt-compensated transmission line and provide synchronized voltages and currents data. Unlike existing methods, the proposed fault location scheme detects faulted section firstly. Then, it finds fault location by using one-end line data and voltage of the shunt-compensator terminal that estimated via other section. Therefore, by assuming the faulted section as a complete line, the proposed algorithm in this paper can be utilized for fault location in lines with incomplete data, too. Other advantages of the proposed scheme over existing methods can be listed as follows:

- It does not require the shunt compensator model as the method in [17] requires.
- The terminal data of the shunt compensator does not utilize as [22]. Therefore, the presented scheme does not require additional measurement devices and communication paths.

In the proposed scheme, after faulted section identification, an optimization problem is developed. Fault location and fault resistance are decision variables of this optimization problem, and the heuristic Particle Swarm Optimization (PSO) algorithm is utilized for calculation them. The proposed scheme can determine precise fault location regardless of shunt-compensator type and shunt compensator location.

2 Description of the Proposed Scheme

As stated before, the proposed method uses synchronized two-end data for fault location. As shown in Fig. 1, the synchronized data prepared by PMUs are transmitted via fiber-optic communications to the fault locator (FL). The proposed scheme calculates the fault location in two steps. In the first step, the faulted section is determined, and the fault location will be calculated in the second step. Subsections 2.1 and 2.2 illustrate two steps of the proposed scheme in detail.

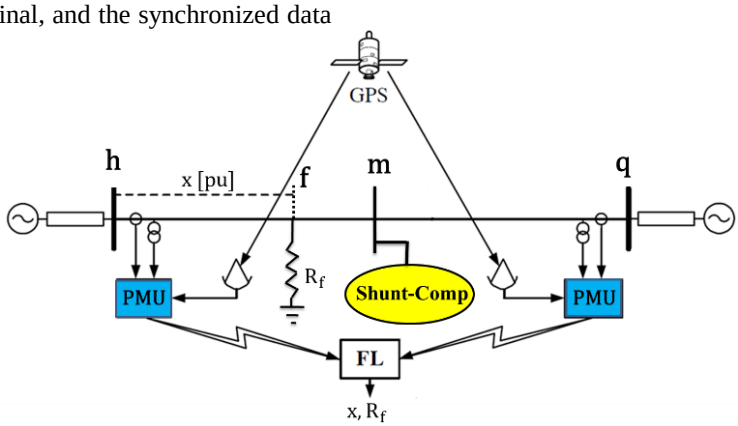

Fig. 1 Schematic diagram for fault location.

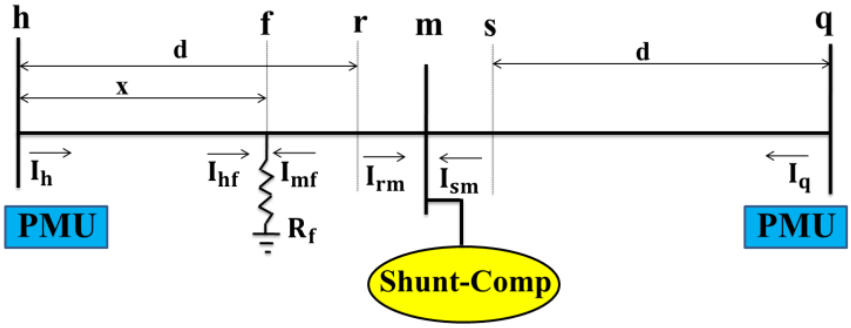

Fig. 2 Schematic of a shunt-compensated line.

2.1 Faulted Section Identification

In this section, a new algorithm based on the presented concept in [28] is proposed for faulted section identification. As illustrated in [28], if there is no fault in the transmission line, the currents at the sending and receiving ends of the line do not have a significant phase difference. After a fault occurs, the currents from both ends of the line will flow toward the fault point, and the phase difference significantly increases. Therefore, the absolute difference of positive-sequence current angles in fault occurrence condition exceeds a threshold value. Hence, the faulted section can be determined by calculating the absolute difference of positive-sequence current angles of two sections of the shunt-compensated line.

Fig. 2 illustrates a shunt-compensated line in detail. Both ends of the line are equipped by PMUs. The left-hand and right-hand sections of the shunt-compensator are notated as S1 and S2, respectively. A fault is assumed to be occurred at the left-hand side of the compensator at distance x from bus h, with fault resistance of R_f.

The following notations are defined:
V_h^a, V_h^b, V_h^c: three-phase voltage phasors at bus h;
I_h^a, I_h^b, I_h^c: three-phase current phasors at bus h;
I_q^a, I_q^b, I_q^c: three-phase current phasors at bus q;
V_f^a, V_f^b, V_f^c: three-phase voltage phasors at fault point;
I^a_{hf}, I^b_{hf}, I^c_{hf}: contribution of the fault current from bus h side;
I^a_{mf}, I^b_{mf}, I^c_{mf}: contribution of the fault current from bus m side;
V^a_{mq}, V^b_{mq}, V^c_{mq}: estimated voltage phasors of bus m using sound section;
V^a_{mh}, V^b_{mh}, V^c_{mh}: estimated voltage phasors of bus m using faulted section;
Z_L: positive-sequence impedance of the line;
L: total length of the line.

In this paper, sequence components are used for finding the fault location. The superscript (i) notates the sequence component. i = 0, 1, and 2 indicate zero, positive and negative sequences, respectively. For example, $V_h^{(1)}$ refers to the positive-sequence voltage at bus h.

To determine the faulted section, the r and s points in sections S1 and S2 are considered in the same distance (d) from line ends and in the vicinity of point m. Therefore, the value of d is assumed to be a number in per unit between 0.9 and 1 ($0.9 < d < 1$). The length of section or $L/2$ is selected as base value. $V_{rh}^{(1)}$ and $V_{sq}^{(1)}$ are the positive-sequence voltages in points r and s that are estimated via bus h and q, respectively. By using the distributed parameters line model between points h and r the estimated voltage $V_{rh}^{(1)}$ can be calculated as follows:

$$V_{rh}^{(1)} = \cosh\left(\gamma^{(1)} d\,\frac{L}{2}\right) \times V_h^{(1)} - Z_c^{(1)} \sinh\left(\gamma^{(1)} d\,\frac{L}{2}\right) \times I_h^{(1)} \quad (1)$$

Similarly, the estimated voltage $V_{sq}^{(1)}$ is calculated from the following equation:

$$V_{sq}^{(1)} = \cosh\left(\gamma^{(1)} d\,\frac{L}{2}\right) \times V_q^{(1)} - Z_c^{(1)} \sinh\left(\gamma^{(1)} d\,\frac{L}{2}\right) \times I_q^{(1)} \quad (2)$$

The equivalent parameters of the transmission line can be calculated as follows:

$$Z_c^{(i)} = \sqrt{\frac{z^{(i)}}{y^{(i)}}}, \quad i = 0,1,2 \quad (3)$$

$$\gamma^{(i)} = \sqrt{z^{(i)} y^{(i)}}, \quad i = 0,1,2 \quad (4)$$

where $Z_c^{(i)}$ and $\gamma^{(i)}$ are the i-th sequence characteristic impedance, and propagation constant of the line, respectively, and $z^{(i)}$ and $y^{(i)}$ are i-th sequence series impedance and shunt admittance of the transmission line per unit length.

Since r and s points are in the vicinity of point m, a short transmission line model can be used for the lines connecting these points to point m. Therefore, by utilizing the following equations, the currents $I_{rm}^{(1)}$ and $I_{sm}^{(1)}$ are calculated:

$$I_{rm}^{(1)} = \frac{V_{rh}^{(1)} - V_{mq}^{(1)}}{(1-d)\,\frac{Z_L}{2}} \quad (5)$$

$$I_{sm}^{(1)} = \frac{V_{sq}^{(1)} - V_{mh}^{(1)}}{(1-d)\frac{Z_L}{2}} \quad (6)$$

The currents $I_h^{(1)}$ and $I_q^{(1)}$ are measured by PMUs; therefore, the absolute difference of the positive-sequence current angles for the section S1 ($\Delta\emptyset_{S1}$) and section S2 ($\Delta\emptyset_{S2}$) can be calculated as follows:

$$\Delta\varnothing_{S1} = \measuredangle I_h^{(1)} - \measuredangle I_{rm}^{(1)} = \measuredangle I_h^{(1)} - \measuredangle\left(V_{rh}^{(1)} - V_{mq}^{(1)}\right) + \measuredangle Z_L \quad (7)$$

$$\Delta\varnothing_{S2} = \measuredangle I_q^{(1)} - \measuredangle I_{sm}^{(1)} = \measuredangle I_q^{(1)} - \measuredangle\left(V_{sq}^{(1)} - V_{mh}^{(1)}\right) + \measuredangle Z_L \quad (8)$$

After occurring a fault at point *r* in S1, the fault point voltage is around the estimated voltage $V_{rh}^{(1)}$. As the fault distance to the bus *h* reduces, the current $I_h^{(1)}$ toward the fault location increases, and the estimated voltage $V_{rh}^{(1)}$ decreases according to (1). Therefore, for occurring a fault at point *f* in the distance *x* from bus *h*, such that $x <$ d, it can be concluded that the estimated voltages $V_{rh}^{(1)}$ and $V_{mh}^{(1)}$ are false and the values of them are less than actual ones, certainly. While the voltages $V_{sq}^{(1)}$ and $V_{mq}^{(1)}$ are equal to the actual values. According to (5) and (6), in occurring a fault at *f*, it can be said that $I_{rm}^{(1)}$ has the direction opposite to the direction demonstrated in Fig. 2. Although $I_h^{(1)}$ and $I_{rm}^{(1)}$ have significant phase difference, $I_q^{(1)}$ and $I_{sm}^{(1)}$ have a small one. Therefore, by calculating the absolute difference of the positive-sequence current angle of the sections S1 and S2, the faulted section can be found.

As proved before, for all fault occurrences in the distance *x* from bus *h*, such that $x < d$, the faulted section can be found correctly. Therefore, to determine the faulted section in fault occurrence at each point of the sections S1 and S2, it is sufficient that the points *r* and s coincide with point m, and the value of *d* is set 1. In this situation, the estimated voltages $V_{rh}^{(1)}$ and $V_{sq}^{(1)}$ are equal to $V_{mh}^{(1)}$ and $V_{mq}^{(1)}$, respectively. Therefore, to calculate the absolute difference of the positive-sequence current angle, the calculation of two voltages $V_{mh}^{(1)}$ and $V_{mq}^{(1)}$ is enough. In this case, Eqs. (7) and (8) are modified as follows:

$$\Delta\varnothing_{S1} = \measuredangle I_h^{(1)} - \measuredangle\left(V_{mh}^{(1)} - V_{mq}^{(1)}\right) + \measuredangle Z_L \quad (9)$$

$$\Delta\varnothing_{S2} = \measuredangle I_q^{(1)} - \measuredangle\left(V_{mq}^{(1)} - V_{mh}^{(1)}\right) + \measuredangle Z_L \quad (10)$$

The value of the phase difference calculated from (9) and (10) for the faulted section is remarkably bigger than the sound section and will exceed a threshold value.

In the occurrence of the faults with high resistance, the absolute difference of the positive-sequence current angles is not a suitable yardstick for determining the faulted section [29]. As shown in Appendix, in case of occurrence Single Line to Ground (SLG) faults, the positive-sequence current angle index is dependent on fault resistance, fault location, and voltages of the ends of the line. However, the negative- and zero- sequence current angles indices do not have any depend on fault resistance and line ends voltage. Therefore, in this paper, the positive-sequence current angle index is used only for symmetrical faults that usually have low fault resistances. Since the negative-sequence current angle index is available for all asymmetrical faults, this index is utilized in this paper for determining faulted section in all asymmetrical faults. This issue is proved analytically in Appendix.

Hence, for asymmetrical faults, the negative-sequence voltages and currents are used in (9) and (10), and the absolute difference of negative-sequence current angles are calculated for two sections. The value of this index for the faulted section is near 180°, and for sound the section is a little more significant than zero. Therefore, by utilizing the positive-sequence current angles for symmetrical faults and negative ones for asymmetrical faults, the faulted section is correctly identifiable, and these indices values for the faulted section are significantly bigger than sound section. Hence, a wide range is accessible for selecting threshold value. However, in this paper, the threshold value for positive and negative indices, similar to [28], has been set to 100°.

2.2 Fault Distance Determination

In this Sub-section the distance of the fault from the beginning bus or *x* is determined. For this, the distributed line model of the transmission line is utilized. After determining the faulted section, the estimated voltage of the shunt-compensator terminal is calculated via the sound section. By using the installed PMU at bus *h*, the three-phase voltage and current phasors and positive-sequences of them are accessible, and the non-positive ones are calculated by the following equations:

$$\begin{bmatrix} V_h^{(0)} \\ V_h^{(2)} \end{bmatrix} = \frac{1}{3}\begin{bmatrix} 1 & 1 & 1 \\ 1 & \alpha^2 & \alpha \end{bmatrix}\begin{bmatrix} V_h^a \\ V_h^b \\ V_h^c \end{bmatrix} \quad (11)$$

$$\begin{bmatrix} I_h^{(0)} \\ I_h^{(2)} \end{bmatrix} = \frac{1}{3}\begin{bmatrix} 1 & 1 & 1 \\ 1 & \alpha^2 & \alpha \end{bmatrix}\begin{bmatrix} I_h^a \\ I_h^b \\ I_h^c \end{bmatrix} \quad (12)$$

where α is defined as $1\angle 120$. By using the distributed parameters line model between *h* and *f*, the following equation is obtained:

$$\begin{bmatrix} V_f^{(i)} \\ I_{hf}^{(i)} \end{bmatrix} = \begin{bmatrix} \cosh\left(\gamma^{(i)} x\frac{L}{2}\right) & -Z_c^{(i)}\sinh\left(\gamma^{(i)} x\frac{L}{2}\right) \\ -\frac{1}{Z_c^{(i)}}\sinh\left(\gamma^{(i)} x\frac{L}{2}\right) & \cosh\left(\gamma^{(i)} x\frac{L}{2}\right) \end{bmatrix}\begin{bmatrix} V_h^{(i)} \\ I_h^{(i)} \end{bmatrix}, \quad i = 0, 1, 2 \quad (13)$$

After calculating the sequence voltages and currents phasors, the three phase values of them at fault point can be calculated by the following equations:

$$\begin{bmatrix} V_f^a \\ V_f^b \\ V_f^c \end{bmatrix} = \begin{bmatrix} 1 & 1 & 1 \\ 1 & \alpha^2 & \alpha \\ 1 & \alpha & \alpha^2 \end{bmatrix} \begin{bmatrix} V_f^{(0)} \\ V_f^{(1)} \\ V_f^{(2)} \end{bmatrix} \tag{14}$$

$$\begin{bmatrix} I_{hf}^a \\ I_{hf}^b \\ I_{hf}^c \end{bmatrix} = \begin{bmatrix} 1 & 1 & 1 \\ 1 & \alpha^2 & \alpha \\ 1 & \alpha & \alpha^2 \end{bmatrix} \begin{bmatrix} I_{hf}^{(0)} \\ I_{hf}^{(1)} \\ I_{hf}^{(2)} \end{bmatrix} \tag{15}$$

In the proposed scheme, the fault type is determined by using the information available at the protection relays. In the following subsections based on fault type, the necessary equations for calculating the contribution of the fault currents from bus m are presented. A three-phase fault model is shown in Fig. 3, and the fault resistance status for the four studied fault types is illustrated in Table 1.

1) *Single-Line-to-Ground Fault (AG)*: For fault between phase A to ground, we have:

$$I_{mf}^a = -I_{hf}^a + \frac{V_f^a}{R_f} \tag{16}$$

$$I_{mf}^b = -I_{hf}^b \tag{17}$$

$$I_{mf}^c = -I_{hf}^c \tag{18}$$

2) *Line-to-Line Fault (BC)*: For phase B to C fault, we have:

$$I_{mf}^a = -I_{hf}^a \tag{19}$$

$$I_{mf}^b = -I_{hf}^b + \frac{\left(V_f^b - V_f^c\right)}{2R_f} \tag{20}$$

$$I_{mf}^c = -I_{hf}^c + \frac{\left(V_f^c - V_f^b\right)}{2R_f} \tag{21}$$

3) *Line-to-Line-to-Ground Fault (BCG)*: For fault between phases B and C to ground, the voltages V_f^b and V_f^c are the same, and we have:

$$I_{mf}^a = -I_{hf}^a \tag{22}$$

$$I_{mf}^b = -I_{hf}^b + \frac{V_f^b}{R_f} \tag{23}$$

$$I_{mf}^c = -I_{hf}^c + \frac{V_f^c}{R_f} \tag{24}$$

4) *Three Phase Symmetrical Fault (ABCG)*: For this type of fault, we have:

$$I_{mf}^a = -I_{hf}^a + \frac{V_f^a}{R_f} \tag{25}$$

$$I_{mf}^b = -I_{hf}^b + \frac{V_f^b}{R_f} \tag{26}$$

$$I_{mf}^c = -I_{hf}^c + \frac{V_f^c}{R_f} \tag{27}$$

As mentioned before, with the availability of the three-phase voltages and currents, the sequence values can be calculated by similar equations as (11) and (12). By having the sequence values, we can calculate the sequence voltages at bus m using the following equation:

$$\left[V_{mh}^{(i)}\right] = \begin{bmatrix} \cosh\left(\gamma^{(i)}(1-x)\frac{L}{2}\right) & Z_c^{(i)}\sinh\left(\gamma^{(i)}(1-x)\frac{L}{2}\right) \end{bmatrix} \begin{bmatrix} V_f^{(i)} \\ I_{fm}^{(i)} \end{bmatrix}, \quad i = 0, 1, 2 \tag{28}$$

After calculating the sequence voltages at bus m, its three-phase voltages will be calculated simply. For actual values of x and R_f, the three-phase estimated voltages at bus m via sound section are approximately equal to the estimated ones via faulted section. Therefore, the difference between the V_{mq}^{abc} and V_{mh}^{abc} in actual fault point is minimum, and an optimization problem is determined as bellow to find the fault distance and resistance:

$$\min_{x, R_f} J = \left[\left(V_{mq}^a - V_{mh}^a\right)^2 + \left(V_{mq}^b - V_{mh}^b\right)^2 + \left(V_{mq}^c - V_{mh}^c\right)^2\right]$$
$$\text{Subject to:} \quad 0 < x < 1, \quad R_f \geq 0 \tag{29}$$

This optimization problem is non-linear and complex, and therefore, an appropriate heuristic method should be used to solve it. There are several heuristic optimization methods, such as Particle Swarm Optimization (PSO), Genetic Algorithm (GA), etc; for solving non-linear

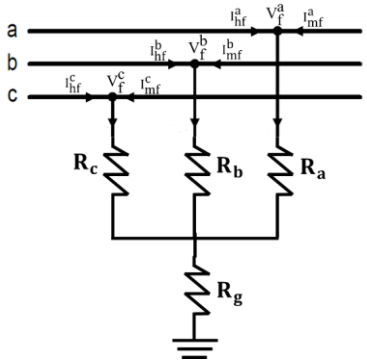

Fig. 3 A comprehensive model for three-phase fault.

Table 1 Different fault types and corresponding fault resistance.

		R_a	R_b	R_c	R_g
Fault Type	AG	zero	inf	inf	R_f
	BC	inf	R_f	R_f	inf
	BCG	inf	zero	zero	R_f
	ABCG	zero	zero	zero	R_f

optimization problems. These methods have their characteristics. Among heuristic optimization methods, PSO has shown seriously encouraging behavior, and this method has been utilized in various fields of optimization alone or in combination with other algorithms [30]. PSO is an algorithm inspired by the social behavior of bird flocking and fish schooling. For the following reasons, among the heuristic methods, PSO has been used to solve the optimization problem in this paper [30-31]:

- Simple, easy to implement, and requires a few adjustable parameters;
- Less affected by initial values;
- Less computational burden and coverage faster than other heuristic methods;
- Fast and its search mechanism is robust and efficient in maintaining diversity.

Algorithm PSO is employed to solve the optimization problem due to its high advantages compared to other methods. In this method, the position and velocity of the particles are updated to achieve the best position (or solution to the optimization problem) [32]. The classic PSO algorithm is utilized in this paper. In this optimization problem, the fault location (x) and fault resistance (R_f) are considered as variables, and therefore, the particles have two dimensions. The velocity (V_{id}) and position (x_{id}) of the particles are updated as follows:

$$V_{id} = w \times V_{id} + c_1 \times r_1 \times (p_{id} - x_{id}) + c_2 \times r_2 \times (g_d - x_{id}), \quad i = 1,2,\ldots,N_s, \quad d = 1,\ 2 \tag{30}$$

$$x_{id} = x_{id} + V_{id} \tag{31}$$

where c_1 and c_2 are acceleration coefficients, r_1 and r_2 are two random numbers in the range [0,1], and N_s is the total number of particles in the swarm, as well. Furthermore, w, p_{id}, and g_d are inertia weight, the best position of each particle, and best position of the swarm, respectively.

In this paper, the initial values of constant parameters (w, c_1, c_2) are selected based on the frequent values given in the literature. The value of w is widely adopted in the range [0.4, 0.9] in literature. Furthermore, in literature, the value of both c_1 and c_2 are generally accepted to be 2 in practical applications of PSO [31]. Based on simulation results, for preventing the algorithm get trapped in local optimal values, the swarm size (N_s) should be selected bigger than 30, while for very big values of N_s, the speed of the algorithm decreases. Therefore, the value of N_s is assumed to be 50. The evaluation results show that by selecting the mentioned values for these parameters, the PSO algorithm has acceptable performance in various conditions, and the parameters are adjusted correctly. Hence the utilized classic PSO algorithm has high efficiency in locating the faults.

3 Evaluation of the Proposed Scheme

A 300 km, 345 kV shunt-compensated transmission line simulates in MATLAB/SIMULINK software to evaluate the proposed method. Fig. 4 illustrates the one-line diagram of the shunt-compensated line, and its parameters are taken from [16]. The simulations are executed by a 2.2 GHz Core i7 CPU with 8 GB of RAM. The proposed scheme is independent of the shunt-compensator model. Therefore, the shunt-compensator can be a STATCOM or an SVC. Both devices are effective in controlling real and reactive power, but STATCOM is faster and more effective in fault situations [33]. Therefore, in the following simulations, it is assumed that a 200 MVA STATCOM is installed at the midpoint of the line.

Two installed PMUs at transmission line ends provide the required data for fault location. To evaluate the proposed scheme different fault types are simulated in several locations of the test system, and some of the simulation results are illustrated in Table 2.

The accuracy of the proposed scheme is evaluated by the percentage error calculated as:

$$\%Error = \frac{|Actual\ Fault\ Location - Estimated\ Fault\ Location|}{Total\ Length\ of\ The\ Line} \times 100 \tag{32}$$

As shown in Table 2, the proposed algorithm in Sub-section 2.1 has been able to correctly determine the faulted section in different fault situations. In columns 4 and 5 of Table 2, for symmetrical faults (ABCG), the absolute differences of the positive-sequence current angles are shown, and negative ones are illustrated for other faults.

After determining faulted section, the voltages and currents data from the PMU-equipped end of this section and estimated voltages of the STATCOM location are utilized by the proposed scheme in Subsection 2.2 for determining fault distance. Columns 7 and 8 of Table 2 show the calculated fault location and its percentage of error, respectively.

As shown in Table 2, the proposed scheme can determine faulted section correctly. Furthermore, in all presented results, the calculated fault location is nearly equal to the actual fault location with high accuracy, and the fault location errors are below 0.29% in all considered fault conditions.

To evaluate the effect of shunt-compensator type, size, and position on the proposed scheme performance, the various fault conditions for different shunt-compensator types, sizes, and locations are simulated and the results are demonstrated in Tables 3 and 4.

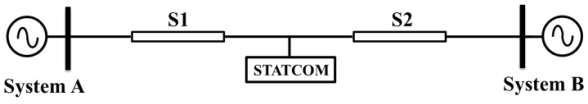

Fig. 4 One-line diagram of the shunt-compensated line.

Table 2 Evaluation of the proposed method under various fault conditions.

Fault type	Fault location [km]	Fault resistance [Ω]	$\Delta\Phi_{S1}$	$\Delta\Phi_{S2}$	Faulted section	Calculated location [km]	Fault location error [%]
AG	5	10	179.70	1.576	S1	5	0.000
		50	179.70	1.576	S1	4.99	0.003
		100	179.70	1.576	S1	4.99	0.003
	75	10	179.70	1.272	S1	75.03	0.010
		50	179.70	1.272	S1	75.03	0.010
		100	179.70	1.272	S1	75.03	0.010
	145	10	179.90	1.293	S1	145.01	0.003
		50	179.90	1.293	S1	144.79	0.070
		100	179.90	1.293	S1	144.13	0.290
	155	10	0.5198	179.3	S2	154.91	0.030
		50	0.5198	179.3	S2	154.82	0.060
		100	0.5198	179.3	S2	154.72	0.090
	225	10	0.2706	179.2	S2	224.97	0.010
		50	0.2706	179.2	S2	224.97	0.010
		100	0.2706	179.2	S2	224.97	0.010
	295	10	0.3074	179.4	S2	295	0.000
		50	0.3074	179.4	S2	295	0.000
		100	0.3074	179.4	S2	295	0.000
BCG	5	10	179.70	1.576	S1	5	0.000
		50	179.70	1.576	S1	5.07	0.023
		100	179.70	1.576	S1	5.08	0.024
	75	10	179.70	1.272	S1	75	0.000
		50	179.70	1.272	S1	75.2	0.070
		100	179.70	1.272	S1	75.2	0.070
	145	10	179.90	1.293	S1	144.81	0.060
		50	179.90	1.293	S1	145.12	0.040
		100	179.90	1.293	S1	145.12	0.040
	155	10	-0.5198	179.3	S2	155.05	0.020
		50	-0.5198	179.3	S2	155.03	0.010
		100	-0.5198	179.3	S2	155.04	0.010
	225	10	-0.2706	179.2	S2	224.93	0.030
		50	-0.2706	179.2	S2	225.12	0.040
		100	-0.2706	179.2	S2	225.1	0.010
	295	10	-0.3074	179.4	S2	294.98	0.006
		50	-0.3074	179.4	S2	295	0.000
		100	-0.3074	179.4	S2	295.1	0.030
BC	5	1	179.70	1.576	S1	5	0.000
		5	179.70	1.576	S1	4.99	0.003
		10	179.70	1.576	S1	4.99	0.003
	75	1	179.70	1.272	S1	75	0.000
		5	179.70	1.272	S1	75	0.000
		10	179.70	1.272	S1	74.99	0.003
	145	1	179.90	1.293	S1	145	0.000
		5	179.90	1.293	S1	144.92	0.026
		10	179.90	1.293	S1	144.86	0.046
	155	1	-0.5198	179.3	S2	154.97	0.010
		5	-0.5198	179.3	S2	154.92	0.026
		10	-0.5198	179.3	S2	154.85	0.05
	225	1	-0.2706	179.2	S2	224.99	0.003
		5	-0.2706	179.2	S2	224.98	0.006
		10	-0.2706	179.2	S2	224.98	0.006
	295	1	-0.3074	179.4	S2	295	0.000
		5	-0.3074	179.4	S2	295	0.000
		10	-0.3074	179.4	S2	295	0.000
ABCG	5	1	156.50	32.80	S1	5	0.000
		5	156.80	33.79	S1	4.99	0.003
		10	157.40	35.94	S1	4.99	0.003
	75	1	152.70	28.72	S1	75	0.000
		5	154.40	31.70	S1	75	0.000
		10	156.10	34.33	S1	75	0.000
	145	1	166.60	42.15	S1	145	0.000
		5	165.00	40.51	S1	144.93	0.023
		10	163.70	39.42	S1	144.87	0.043
	155	1	28.100	152.9	S2	154.97	0.010
		5	29.940	154.7	S2	154.92	0.026
		10	30.260	154.7	S2	154.87	0.043
	225	1	30.970	155.8	S2	224.99	0.003
		5	30.420	155.7	S2	224.98	0.006
		10	30.790	155.7	S2	224.98	0.006
	295	1	37.790	162.3	S2	295	0.000
		5	37.160	161.9	S2	295	0.000
		10	36.620	161.6	S2	295	0.000

Table 3 The effect of shunt-compensator location on the proposed scheme.

Comp. location [km]	Fault type, Resistance [Ω]	Fault Loc. [km]	Calculated Loc. [km]	Error [%]
100	AG, 100	5	4.99	0.003
		145	144.91	0.03
		295	295	0.0
	BC, 10	5	4.99	0.003
		145	145	0.0
		295	295	0.0
	ABCG, 10	5	5	0.0
		145	144.97	0.01
		295	295	0.0
150	AG, 100	5	4.99	0.003
		145	144.13	0.29
		295	295	0.0
	BC, 10	5	4.99	0.003
		145	144.86	0.046
		295	295	0.0
	ABCG, 10	5	4.99	0.003
		145	144.87	0.043
		295	295	0.00
200	AG, 100	5	4.99	0.003
		145	145.05	0.016
		295	295	0.0
	BC, 10	5	5	0.0
		145	145	0.0
		295	295	0.0
	ABCG, 10	5	5	0.0
		145	145	0.0
		295	295	0.0

Table 4 The effect of shunt-compensator capacity and type on the proposed scheme.

Comp. Cap. [MVA]	Fault Type	Fault Res. [Ω]	Fault Loc. [km]	STATCOM		SVC	
				Calc. Loc. [km]	Error [%]	Calc. Loc. [km]	Error [%]
100	AG	100	5	4.99	0.003	4.99	0.003
			145	144.13	0.29	144.13	0.29
			295	295	0.0	295	0.0
	BC	10	5	4.99	0.003	4.99	0.003
			145	144.86	0.046	144.80	0.066
			295	295	0.00	295	0.00
	ABCG	10	5	4.99	0.003	4.99	0.003
			145	144.87	0.043	144.83	0.056
			295	295	0.00	295	0.00
200	AG	100	5	4.99	0.003	4.99	0.003
			145	144.13	0.29	144.13	0.29
			295	295	0.0	295	0.0
	BC	10	5	4.99	0.003	4.99	0.003
			145	144.86	0.046	144.80	0.066
			295	295	0.00	295	0.0
	ABCG	10	5	4.99	0.003	4.99	0.003
			145	144.87	0.043	144.83	0.056
			295	295	0.00	295	0.00
300	AG	100	5	4.99	0.003	4.99	0.003
			145	144.13	0.29	144.13	0.29
			295	295	0.0	295	0.00
	BC	10	5	4.99	0.003	4.99	0.003
			145	144.86	0.046	144.80	0.066
			295	295	0.00	295	0.0
	ABCG	10	5	4.99	0.003	4.99	0.003
			145	144.87	0.043	144.83	0.056
			295	295	0.00	295	0.00

As mentioned previously, the shunt compensator usually installs at the mid-point of the line. For evaluation of the effect of shunt-compensator location, three different locations are assumed for STATCOM installation, and the simulation results are illustrated in Table 3. As can be seen in this table, for various shunt-compensator locations, the proposed scheme can calculate the exact fault location. The presented results in this table show that the location of the shunt-compensator has almost no effect on the accuracy of the fault location. As expected and as can be seen in Table 4, the capacity and type of shunt compensator do not affect the performance of the proposed scheme, too.

4 Effect of PMUs' Data Quality

The evaluations in the previous section were performed assuming the received voltage, and current phasors from PMUs are ideal and error-free. The effect of PMUs' data quality on the performance of the proposed scheme is investigated in this section. In literature, the data quality issue of PMUs is categorized into three qualities, involving data accuracy, data loss and, data latency [34].

The performance of PMU in measuring, digitalizing, and packaging data is defined as data accuracy. In standard C37. 118. 1.2011[35], the data quality is quantified by utilizing the total vector error (TVE) index. The maximum acceptable TVE is 1%; this value corresponds to 0.57 degrees for 60 HZ power systems. In order to explore the effect of data accuracy on the performance of the proposed scheme, the angle of received phasors from PMUs, have been randomly drifted from the measured values up to the standard limit (0.57 degrees) before utilizing them in the proposed scheme. The evaluation results for a few fault conditions in the test system, by considering the mentioned data error, are shown in Table 5. These simulations are tried 100 times, and the minimum and maximum values of the calculated fault locations in these 100 attempts are presented in columns 3 and 5 of Table 5, respectively. The faulted section has been determined correctly in all fault situations. As shown in this table, the proposed fault location scheme can locate the faults with high accuracy in these conditions, too.

Loss of PMU data may affect PMU-based applications. However, observations show that 95% of data loss involves only 1, 2, or 3 continuous packet losses, and a large amount of packet is less likely to occur [34]. Fault location problems utilize post-fault data for finding the location of the fault. PMUs send the measured data packets in each cycle [36], and therefore, in the data loss conditions, the fault location must be determined by utilizing the voltages and currents data that probably measured several cycles (up to 4 cycles) after fault occurrence. According to the simulation results, the proposed fault location scheme is able to do this. So, in the majority of data loss issues (almost 95% of them), the location of the fault can be found by the proposed scheme.

As mentioned before, the data latency created by communication links can affect the data quality of PMUs. These delays may vary in different time periods [34]. Although in this situation, the data chain is complete, due to the data latency, the delivery of data packets to the fault locator is delayed more than typical delay values. Therefore, if the amount of delay is acceptable for a system, the proposed fault location scheme can determine the fault location accurately.

5 Comparative Assessment

In this section, a comparative assessment between the proposed scheme and some existing methods is carried out. As mentioned before, the fault location methods for shunt-compensated transmission lines have presented in a few articles. Although the presented method in [16] is accurate and does not require the shunt compensator model, this method requires a high sampling rate, and its implementation is very costly. The proposed method in [17] requires the shunt-compensator model for fault location. Requiring to shunt-compensator model for the following reasons can affect the efficiency of the fault location methods.

- The shunt-compensator model is only available in some shunt-compensators such as shunt reactor and due to the variable operation point and uncertainty; a fixed model is not available for other shunt-compensators such as SVC, STATCOM, etc.
- The protection system of the shunt-compensator will likely shut down the compensator in some internal or external fault cases. Disconnecting of the compensator and its disconnection time are among the uncertainties in the shunt compensator model.
- Modeling of some shunt-compensators, such as STATCOM, considering practical constraints and during the fault situations is a difficult and sophisticated issue.
- By utilizing the shunt-compensator model, the errors resulted from modeling of the shunt-

Table 5 The impact of the PMUs' data quality on the proposed scheme performance.

Fault type, Resistance [Ω]	Fault Loc. [km]	Min calculated Loc. [km]	Error [%]	Max. calculated Loc. [km]	Error [%]
AG, 100	5	4.23	0.256	5.86	0.286
	145	143.36	0.546	146.52	0.491
	295	294.73	0.09	295.29	0.096
BC, 10	5	4.49	0.17	5.29	0.096
	145	143.6	0.46	146.33	0.443
	295	294.88	0.04	295.32	0.106
BCG, 100	5	4.42	0.193	5.47	0.156
	145	143.53	0.49	146.35	0.45
	295	294.81	0.063	295.31	0.103
ABCG, 10	5	4.98	0.006	5.10	0.033
	145	144.99	0.003	145.02	0.006
	295	294.01	0.030	295.02	0.006

Table 6 Comparative assessment of the proposed method with a number of similar methods.

Ref. No.	Calculated variables	Requiring to Shunt_comp. model	Requiring to Shunt_comp. terminal data	Shunt_comp. type	Max. error [%]
[16]	x, R_f	No	No	All types	0.0454
[17]	x	Yes	No	Shunt reactor	Below 1%
[22]	x, Apparent impedance	No	Yes	SVC	Not available
Proposed scheme	x, R_f	No	No	All types	0.29

compensator can affect the accuracy of the fault location method.

Therefore, the requirement to the shunt-compensator model can be considered as a limitation for the presented method in [17].

The presented method in [22] utilizes the terminal data of the shunt compensator and requires additional measurement devices and communication paths.

Comparative assessment of the proposed scheme with similar methods has been summarized in Table 6. In the proposed scheme in this paper, the faulted section is determined first, so as the search area shrinks, the accuracy of the method in locating the fault increases. The proposed method does not require the shunt-compensated model and can be utilized for different shunt-compensated lines. Furthermore, the proposed scheme can determine accurate fault location without utilizing shunt-compensator terminal data.

6 Conclusion

In this paper, an accurate fault location scheme for shunt-compensated transmission lines is proposed. Based on the gathered data from PMUs, the proposed scheme determines the faulted section firstly and then detects fault location by solving an optimization problem. In this paper, by presenting the absolute difference of negative-sequence current angle, an effective approach for identifying faulted section is proposed. The accuracy of the proposed scheme is increased by determining faulted section and limiting the search area. The proposed scheme does not require any data from the shunt-compensator location and does not dependent on the shunt-compensator model. Furthermore, the shunt-compensator location, type, and capacity do not any impact on the fault location accuracy. The efficiency of the proposed method is proved by simulating different fault conditions in the test system. Furthermore, the proposed scheme can attain up to 99.71% accuracy for all studied cases.

Appendix

As mentioned in Section 2, the presented idea in [28], is utilized for identifying the faulted section. In this Appendix, it is analytically shown that the positive-sequence current angle index (presented in [28]) does not operate correctly in some high resistance faults. In addition, it is approved that the negative-sequence current angle index has high efficiency in high resistance fault occurrences.

Fig. A1 shows a transmission line with a fault at x distance from bus S, where x is in p.u. In case of fault occurrence at any point of the transmission line, currents from both ends of the line will flow toward the fault point. The sequence networks are connected in series for SLG fault, as shown in Fig. A2.

The following notations are used in Fig. A2:

E_S, E_R: Thevenin voltage seen from bus S and R, respectively;

$Z_L^{(i)}$: i-th sequence impedance of the line;

$Z_S^{(i)}$: i-th sequence Thevenin impedance seen from bus S;

$Z_R^{(i)}$: i-th sequence Thevenin impedance seen from bus R;

$I_S^{(i)}$, $I_R^{(i)}$: i-th sequence currents flowing toward fault point from buses S and R, respectively;

$I_f^{(i)}$: i-th sequence fault current;

R_f : Fault resistance;

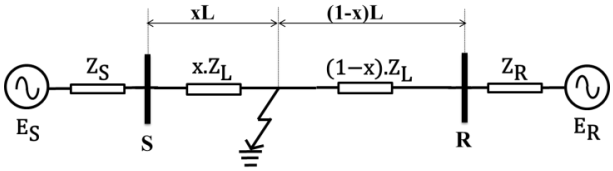

Fig. A1 Single line diagram of a sample transmission line.

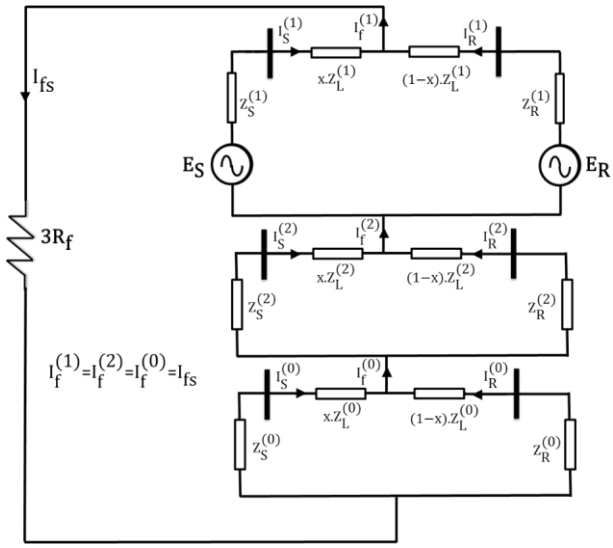

Fig. A2 Sequence network connection under SLG fault condition.

As shown in Fig. A2, the sequence fault currents $I_f^{(1)}$, $I_f^{(2)}$, and $I_f^{(0)}$ are equal together, and therefore, these are shown as I_{fs} in the next equations. Positive, negative, and zero sequence currents that flow from ends of the line toward fault location have opposite direction. After a brief analysis, the sequence of fault currents shown in Fig. A2 is calculated as follows:

$$I_{fs}=\frac{Z_t^{(1)}\left(\frac{E_S}{x.Z_L^{(1)}+Z_S^{(1)}}+\frac{E_R}{(1-x).Z_L^{(1)}+Z_R^{(1)}}\right)}{Z_t^{(0)}+Z_t^{(1)}+Z_t^{(2)}+3R_f} \tag{A1}$$

where

$$Z_t^{(i)}=\frac{\left(x.Z_L^{(i)}+Z_S^{(i)}\right)\left((1-x).Z_L^{(i)}+Z_R^{(i)}\right)}{Z_S^{(i)}+Z_R^{(i)}+Z_L^{(i)}},$$
$$i=0,1,2 \tag{A2}$$

Also, for the sequence currents I_S and I_R, we have:

$$I_S^{(1)}=\frac{E_S-E_R+\left((1-x).Z_L^{(1)}+Z_R^{(1)}\right).I_{fs}}{Z_S^{(1)}+Z_R^{(1)}+Z_L^{(1)}} \tag{A3}$$

$$I_R^{(1)}=\frac{E_R-E_S+\left(x.Z_L^{(1)}+Z_S^{(1)}\right).I_{fs}}{Z_S^{(1)}+Z_R^{(1)}+Z_L^{(1)}} \tag{A4}$$

$$I_S^{(i)}=\frac{Z_R^{(i)}+(1-x).Z_L^{(i)}}{Z_S^{(i)}+Z_R^{(i)}+Z_L^{(i)}}.I_{fs},\quad i=0,2 \tag{A5}$$

$$I_R^{(i)}=\frac{Z_S^{(i)}+x.Z_L^{(i)}}{Z_S^{(i)}+Z_R^{(i)}+Z_L^{(i)}}.I_{fs},\quad i=0,2 \tag{A6}$$

$$K_S^{(i)}=\frac{Z_R^{(i)}+(1-x).Z_L^{(i)}}{Z_S^{(i)}+Z_R^{(i)}+Z_L^{(i)}},\quad i=0,2 \tag{A7}$$

$$K_R^{(i)}=\frac{Z_S^{(i)}+x.Z_L^{(i)}}{Z_S^{(i)}+Z_R^{(i)}+Z_L^{(i)}},\quad i=0,2 \tag{A8}$$

$$I_S^{(i)}=K_S^{(i)}.I_{fs},\quad i=0,2 \tag{A9}$$

$$I_R^{(i)}=K_R^{(i)}.I_{fs},\quad i=0,2 \tag{A10}$$

$$\measuredangle I_S^{(i)}=\measuredangle K_S^{(i)}+\measuredangle I_{fs},\quad i=0,2 \tag{A11}$$

$$\measuredangle I_R^{(i)}=\measuredangle K_R^{(i)}+\measuredangle I_{fs},\quad i=0,2 \tag{A12}$$

The absolute difference of the i-th-sequence current angles ($\Delta\emptyset^{(i)}$) can be calculated from the following equation for zero, positive, and negative sequence, respectively.

$$\Delta\varnothing^{(i)}=\measuredangle I_R^{(i)}-\measuredangle I_S^{(i)}=\left(180+\measuredangle I_R^{(i)}\right)-\measuredangle I_S^{(i)},$$
$$i=0,1,2 \tag{A13}$$

As can be seen from (A3), (A4), and (A13), the absolute difference of the positive-sequence current angle ($\Delta\emptyset^{(1)}$) is dependent on I_{fs}, and hence this index is dependent on fault resistance, fault location, and voltages of the ends of the line. The value of the absolute difference of the non-positive-sequence current angles ($\Delta\emptyset^{(2)}$ and $\Delta\emptyset^{(0)}$) can be calculated as follow:

$$\Delta\varnothing^{(i)}=\left(180+\measuredangle I_R^{(i)}\right)-\measuredangle I_S^{(i)}$$
$$=180+\measuredangle K_R^{(i)}-\measuredangle K_S^{(i)},\qquad i=0,2 \tag{A14}$$

As can be seen in (A14), unlike $\Delta\emptyset^{(1)}$, the values of $\Delta\emptyset^{(2)}$ and $\Delta\emptyset^{(0)}$ are entirely independent of I_{fs} and consequently independent of R_f. Furthermore, these values only dependent on fault location (x). Therefore, as explained in Section 2, the absolute difference of the negative-sequence current angles is more proper than the positive one in the case of asymmetrical faults that often have high fault resistance.

References

[1] M. M. Saha, J. Izykowski, and E. Rosolowski, *Fault location on power networks*. Springer-Verlag: London, 2010.

[2] D. Novosel, B. Bachmann, D. Hart, and M. M. Saha, "Algorithm for locating faults on series compensated lines using neural network and deterministic methods," *IEEE Transactions on Power Delivery*, Vol. 11, No. 4, pp. 1728–1736, 1996.

[3] M. B. Djuric, Z. M. Radojevic, and V. V. Terzija, "Distance protection and fault location utilizing only phase current phasors," *IEEE Transactions on Power Delivery*, Vol. 13, No. 4, pp. 1020–1026, 1998.

[4] Q. Zhang, Y. Zhang, W. Song, and Y. Yu, "Transmission line fault location for phase-to-earth fault using one-terminal data," in *IEE Proceedings-Generation, Transmission and Distribution*, Vol. 146, No. 2, pp. 121–124, 1999.

[5] T. Kawady and J. Stenzel, "A practical fault location approach for double circuit transmission lines using single end data," *IEEE Transactions on Power Delivery*, Vol. 18, No. 4, pp. 1166–1173, 2003.

[6] J. Lzykowski, E. Rosolowski, and M. M. Saha, "Locating faults in parallel transmission lines under availability of complete measurements at one end," in *IEE Proceedings-Generation, Transmission and Distribution*, Vol. 151, No. 2, pp. 268–273, 2004.

[7] A. Ghorbani and H. Mehrjerdi, "Accurate fault location algorithm for shunt-compensated double circuit transmission lines using single end data," *International Journal of Electrical Power & Energy Systems*, Vol. 116, No. 1, pp. 861–867, 2020.

[8] A. Johns and S. Jamali, "Accurate fault location technique for power transmission lines," in *IEE Proceedings C (Generation, Transmission and Distribution)*, Vol. 137, No. 6, pp. 395-402, 1990.

[9] M. Kezonovic and P. Perunicic, "Automated transmission line fault analysis using synchronized sampling at two ends," *IEEE Transactions on Power Delivery*, Vol. 11, No. 1, pp. 441–447, 1996.

[10] I. Zamora, J. F. Minabres, and A. J. Mazon, "Fault location on two-terminal transmission lines based on voltages," *IEE Proceedings-Generation, Transmission and Distribution*, Vol. 143, No. 1, pp. 1–6, 1996.

[11] S. M. Brahma and A. A. Girgis, "Fault location on a transmission line using synchronized voltage measurements," *IEEE Transactions on Power Delivery*, Vol. 19, No. 4, pp. 1619–1622, 2004.

[12] Y. Liao and S. Elangovan, "Unsynchronised two-terminal transmission lines fault location without using line parameters," *IEE Proceedings-Generation, Transmission and Distributi*on, Vol. 153, No. 6, pp. 639–643, 2006.

[13] Y. Liao and M. Kezonovic, "Optimal estimate of transmission line fault location considering measurement errors," *IEEE Transactions on Power Delivery*, Vol. 22, No. 3, pp. 1335–1341, 2007.

[14] Y. Liao, "Fault location for single-circuit line based on bus-impedance matrix utilizing voltage measurement," *IEEE Transactions on Power Delivery*, Vol. 23, No. 2, pp. 609–617, 2008.

[15] Y. Liao and N. Kang, "Fault location algorithms without utilizing line parameters based on distributed parameter line model," *IEEE Transactions on Power Delivery*, Vol. 24, No. 2, pp. 579–584, 2009.

[16] M. Ghazizadeh-Ahsaee and J. Sadeh, "Accurate fault location algorithm for transmission lines in the presence of shunt-connected flexible AC transmission system devices," *IET Generation, Transmission and Distribution*, Vol. 6, No. 3, pp. 247–255, 2012.

[17] S. Hussain and A. H. Osman, "Fault location on series and shunt-compensated lines using unsynchronised measurement," *Electric Power Systems Research*, Vol. 116, No. 1, pp. 166–173, 2014.

[18] M. G. Adamiak, A. P. Apostolov and M. M. Begovic, "Wide area protection—technology and infrastructures," *IEEE Transactions on Power Delivery*, Vol. 21, No. 2, pp. 601–609, 2006.

[19] J. A. Jiang, J. Yang, Y. Lin, C. Liu, and J. Ma, "An adaptive PMU based fault location/detection technique for transmission lines," *IEEE Transactions on Power Delivery*, Vol. 15, No. 2, pp. 486–493, 2000.

[20] C. Yu, C. Liu, S. Yu, and J. A. Jiang, "A new PMU-based fault location algorithm for series compensated lines," *IEEE Transactions on Power Delivery*, Vol. 17, No. 1, pp. 33–46, 2002.

[21] X. Jiao and Y. Liao, "Accurate fault location for untransposed/transposed transmission lines using sparse wide area measurement," *IEEE Transactions on Power Delivery*, Vol. 31, No. 4, pp. 1797–1805, 2016.

[22] N. Khoa and D. D. Tung, "Locating fault on transmission line with static Var compensator based on phasor measurement unit," *Energies*, Vol. 11, No. 9, 2018.

[23] N. G. Hingorani and L. Gyugyi, *Understanding FACTS: Concepts & technology of flexible AC transmission systems*. New York: Wiley, Nov. 1999.

[24] B. T. Ooi, M. Kazerani, R. Marceau, and G. Joos, "Mid-point siting of FACTS devices in transmission lines," *IEEE Transactions on Power Delivery*, Vol. 12, No. 4, pp. 1717–1722, 1997.

[25] M. H. Haque, "Optimal location of shunt FACTS devices in long transmission lines," in *IEE Proceedings-Generation, Transmission and Distribution*, Vol. 147, No. 4, pp. 218–222, 2000.

[26] A. Ghorbani, M. Khederzadeh, and B. Mozafari, "Impact of SVC on the protection of transmission lines," *International Journal of Electrical Power & Energy Systems*, Vol. 42, No. 1, pp. 702–709, 2012.

[27] T. S. Sidhu, R. K. Varma, P. K. Gangadharan, F. A. Albasri, and G. R. Ortiz, "Performance of distance relays on shunt-FACTS compensated transmission lines," *IEEE Transactions on Power Delivery*, Vol. 20, No. 3, pp. 1837–1845, 2005.

[28] M. M. Eissa, M. E. Masoud, and M. M. Elanvar, "A novel back up wide area protection technique for power transmission grids using phasor measurement unit," *IEEE Transactions on Power Delivery*, Vol. 25, No. 1, pp. 170–278, 2010.

[29] S. Mirhosseini and M. Akhbari, "Wide area backup protection algorithm for transmission lines based on fault component complex power," *International Journal of Electrical Power & Energy Systems*, Vol. 83, pp. 1–6, 2016.

[30] C. P. Lim, L. C. Jian, and S. Dehuri, *Innovations in swarm intelligence*. Springer-Verlag: London, 2009.

[31] A. R. Jordehi and J. Jasni, "Parameter selection in particle swarm optimization: A survey," *Journal of Experimental & Theoretical Artificial Intelligence*, Vol. 25, No. 4, pp. 527–542, 2013.

[32] A. W. Mohemmed, N. C. Sahoo, and T. K. Geok, "Solving shortest path problem using particle swarm optimization," *Applied Soft Computing*, Vol. 8, No. 4, pp. 1643–1653, 2008.

[33] T. Tran, X. Zha, and N. Le, "Performance comparison between STATCOM and SVC to enhance power system stability," *Applied Mechanics and Materials*, Vols. 446–447, pp. 759–763, 2014.

[34] A. G. Phadke, P. Wall, L. Ding, and V. Terzija, "Data quality issues for synchrophasor applications part I: A review," *Journal of Modern Power Systems and Clean Energy*, Vol. 4, No. 3, pp. 342–352, 2016.

[35] *IEEE standard for synchrophasor measurements for power systems*, IEEE Std C37.118.1-2011 (Revision of IEEE Std C37.118-2005), Dec. 2011.

[36] A. G. Phadke, P. Wall, L. Ding, and V. Terzija, "Improving the performance of power system protection using wide area monitoring systems," *Journal of Modern Power Systems and Clean Energy*, Vol. 4, No. 3, pp. 319–331, 2016.

M. Ahmadinia was born in Neyshabour, Iran in 1984. He received the B.Sc. from the Shahid Rajaee University of Tehran and M.Sc. from the Ferdowsi University of Mashhad both in Electrical Engineering in 2006 and 2008, respectively. He is currently pursuing a Ph.D. degree at Ferdowsi University of Mashhad, Mashhad, Iran. He is interested in power system protection, power system dynamics, and FACTS devices.

J. Sadeh was born in Mashhad, Iran in 1968. He received the B.Sc. and M.Sc. with honor both in Electrical Engineering from Ferdowsi University of Mashhad, Mashhad, Iran in 1990 and 1994, respectively, and obtained his Ph.D. in Electrical Engineering from Sharif University of Technology, Tehran, Iran with the collaboration of the Electrical Engineering Laboratory of the Institut National Polytechnique de Grenoble (INPG), France in 2001. He is currently a Professor in the Department of Electrical Engineering, Ferdowsi University of Mashhad, Mashhad, Iran. His research interests are power system protection, dynamics and operation.